Eur Biophys J (2011) 40:117–129
DOI 10.1007/s00249-010-0630-y

ORIGINAL PAPER

An alternative flexible conformation of the *E. coli* HUβ_2 protein: structural, dynamics, and functional aspects

Norbert Garnier · Karine Loth · Franck Coste · Rafal Augustyniak · Virginie Nadan · Christian Damblon · Bertrand Castaing

Received: 9 June 2010 / Revised: 15 September 2010 / Accepted: 20 September 2010 / Published online: 10 October 2010

Abstract The histone-like HU protein is the major nucleoid-associated protein involved in the dynamics and structure of the bacterial chromosome. Under physiological conditions, the three possible dimeric forms of the *E. coli* HU protein (EcHUα_2, EcHUβ_2, and EcHU$\alpha\beta$) are in thermal equilibrium between two dimeric conformations ($N_2 \leftrightarrow I_2$) varying in their secondary structure content. High-temperature molecular dynamics simulations combined with NMR experiments provide information about structural and dynamics features at the atomic level for the N_2 to I_2 thermal transition of the EcHUβ_2 homodimer. On the basis of these data, a realistic 3D model is proposed for the major I_2 conformation of EcHUβ_2. This model is in agreement with previous experimental data.

Keywords Histone-like HU protein · Thermal stability · Structure flexibility · Molecular dynamics simulation · NMR

The manually built model of EcHUβ_2 is accessible at PMDB id: PM0076052.

Electronic supplementary material The online version of this article (doi:10.1007/s00249-010-0630-y) contains supplementary material, which is available to authorized users.

N. Garnier · K. Loth · F. Coste · R. Augustyniak · V. Nadan · C. Damblon · B. Castaing (✉)
Centre de Biophysique Moléculaire (CNRS, UPR4301), University of Orléans, rue Charles Sadron, 45071 Orléans cedex 02, France
e-mail: castaing@cnrs-orleans.fr

R. Augustyniak
Department of Physical Chemistry, Faculty of Pharmacy, Medical University of Warsaw, Banacha 1 Street, 02-097 Warsaw, Poland

Present Address:
R. Augustyniak
Département de Chimie Associé au CNRS (UMR7203), Ecole Normale Supérieure, 24 rue Lhomond, 75231 Paris Cedex 05, France

Present Address:
C. Damblon
Chimie Biologique Structurale, Institut de Chimie, Sart-Tilman (B6c), Université de Liège, 4000 Liège, Belgium

Introduction

DNA replication, transcription, recombination, and repair depend on the precise topologies and structural dynamics of the chromosomal DNA, which itself varies in response to environmental changes (Echols 1990). For this purpose, prokaryotes have evolved molecular mechanisms involving nucleoid-associated proteins assigned to compact and to organise the bacterial chromosome in a high-order structured nucleoproteic particle, the nucleoid (Pettijohn 1996). Among these proteins, the bacterial HU protein is the most abundant ($3–5 \times 10^4$ molecules/bacterium) and the best documented. HU is a small dimeric basic protein (2×10 kDa, pI = 10.5) and, similarly to eukaryotic histones, it wraps DNA in a non-specific manner, promoting high-order DNA super-structures (Pettijohn 1996; Rouviere-Yaniv et al. 1979). HU is also able to form high-affinity complexes with DNA containing sharp bends, kinks, branched and bulged structures, and single-strand breaks and loops (Bonnefoy et al. 1994; Castaing et al. 1995; Lavoie et al. 1996; Lyubchenko et al. 1997; Pontiggia et al. 1993). Because of its peculiar DNA binding properties, HU is involved in various physiological and accommodation cellular processes, for example replication initiation, DNA protection against irradiation, site-specific recombination,

and DNA transcription modulation in response to heat and cold shock stress, anaerobiosis, acid stress, high osmolarity, and SOS induction (Oberto et al. 1994, 2009).

Whereas in enteric bacteria such as *E. coli*, HU is present as two homodimers and one heterodimer, in other eubacteria, HU is generally present as a single homodimer. In *E. coli*, the *hupA* and *hupB* genes code for the HUα and HUβ polypeptide chains, respectively. The HU chains combine to form EcHUα_2, EcHUβ_2, and EcHU$\alpha\beta$ dimers (Ramstein et al. 2003). The HU pool composition is correlated with differential expression of the *hup* genes (Claret and Rouviere-Yaniv 1996, 1997). Disruption of both genes strongly affects the growth of the double mutant strain and is associated with perturbations of cell division, heat-lethal phenotype, and hyper-sensitivity to ionising radiation (Boubrik and Rouviere-Yaniv 1995; Li and Waters 1998). After a cold shock, the *hupA* gene is repressed while the *hupB* gene is over-expressed, indicating that EcHUβ_2 is required for *E. coli* cold shock adaptation (Giangrossi et al. 2002; Gualerzi et al. 2003).

Genetic studies and DNA binding properties of HU species suggest that each *E. coli* HU dimer has a different biological purpose (Oberto et al. 2009). In previous work, we described the use of differential scanning calorimetry (DSC), circular dichroism (CD), and crystal structure analysis to show that each *E. coli* dimer also has different thermal properties which might be related to their respective functional purposes (Ramstein et al. 2003). Unlike the other HU proteins which melt in a single step ($N_2 \leftrightarrow 2D$), we showed that the three *E. coli* dimers follow a two-step mechanism ($N_2 \leftrightarrow I_2 \leftrightarrow 2D$). The N_2 species corresponds to a dimer with a compact structure (Fig. 1S) and the I_2 species to a more flexible dimer having lost native structural elements. Each *E. coli* dimer is constituted by three subdomains: a very flexible and thermally unstable part (the "arms" of the dimer) which do not contribute to the stability of the protein body, and a very compact and stable part (the "body" of the dimer) constituted by two energetic and structural subdomains (the α-helix and β-strand-rich subdomains) (Fig. 1S). CD experiments indicated that during the N_2 to I_2 thermal transition, the structure of the α-helix-rich subdomain of the protein body partly changes. The $N_2 \leftrightarrow I_2$ equilibrium is thought to be of central importance in the *E. coli* HU system, because N_2 versus I_2 conformations of each dimer co-exist under physiological conditions (37°C, 0.2 M NaCl). Although most of the other HU proteins studied so far (from thermophile or mesophile bacteria) do not have different conformations, unexpectedly, an alternate highly flexible conformation of the hyperthermostable HU protein from *Thermotoga maritima* (HUtmar) has also been described but its biological significance remains unclear (Durney et al. 2004). Previously, we have proposed that I_2 might be required in *E. coli* for the HU chain exchange which enables heterodimer formation from both preformed homodimers without the need for the non-physiological denatured monomer states. This suggestion is based on the observation that, in vitro, the formation of the *E. coli* heterodimer is drastically inhibited by low temperature, a condition for which *E. coli* homodimers are essentially present in their N_2 conformation (Ramstein et al. 2003). Interestingly, the I_2 molecular state is the predominant conformation of EcHUβ_2 under physiological conditions which can be connected to its role in *E. coli* cold-shock adaptation and its propensity to oligomerise (Giangrossi et al. 2002; Oberto et al. 2009; Rouviere-Yaniv and Kjeldgaard 1979).

In this work, we performed high-temperature molecular dynamics (MD) simulations and preliminary NMR analysis to obtain structural and dynamics insights into the $N_2 \leftrightarrow I_2$ conformational transition of EcHUβ_2. The main objective of this work was to propose a structural model for the I_2 conformation of EcHUβ_2 and the possible structural remodelling pathway associated with the N_2 to I_2 transition of EcHUβ_2.

Materials and methods

Proteins

The labelled and unlabelled EcHUβ_2 homodimers were prepared as previously described (Coste et al. 1999; Ramstein et al. 2003). Isotope labelling (^{15}N or $^{15}N/^{13}C$) of the protein was performed as previously described (Marley et al. 2001). Isotopic labelling of the purified, labeled protein was 99.7% (estimated by MaldiToff mass spectroscopy). The protein concentration was estimated by the Biuret method. After concentration (up to 90 mg/ml), each protein sample (in 20 mM Na phosphate, 0.2 M NaCl, and 0.05 mM DTT) was flash-cooled in liquid nitrogen and stored at −80°C. The final concentration of the isotope-labelled NMR samples was 1.54 mM in 400 µl (95% H_20/5% D_2O) of the previous buffer, containing DSS as internal reference, at pH 7.6. Unlabelled EcHUβ_2 was used to monitor oligomerization of the protein in the presence of the dimethylsuberimidate (DMS) cross-linker (see supplementary Information).

Construction of a 3D model of EcHUβ_2 used as starting model for simulation

The biologically relevant EcHUα_2 homodimer was created by applying the transformation generated by the crystallographic two-fold rotation axis parallel to c from the coordinates of the PDB id: 1MUL structure (Ramstein et al. 2003). The flexible arms, missing in the crystal structure, were modelled from the protein residues 56–73

of the Anabaena sp. HU/DNA complex crystal structure (PDB id: 1P71) (Swinger et al. 2003). LSQKAB software was used to fit the AsHU β-strand 2 and 3 residues with the corresponding residues of EcHU in order to correctly insert the AsHU arms on the EcHUα_2 protein body. The WHAT IF web interface was then used to mutate the residues and to model the missing side chains to obtain a complete EcHUα_2 homodimer model. The EcHUβ_2 homodimer was created by mutating the complete EcHUα_2 model using the WHAT IF server. Finally, Procheck software was used to assess the stereochemical quality of the models. Hydrogen atoms were added and the homodimer model of EcHUβ_2 was minimised (PMDB id: PM0076052, Fig. 1Sc).

Molecular dynamics simulations

The minimised structure of EcHUβ_2 was then placed in a rectangular box of explicit water molecules. The oxygen atoms of water molecules less than 2.4 Å from any atoms of the homodimer were deleted. To ensure the neutrality of the system, counter ions were added (23 Cl^- and 15 Na^+). The resulting system, made up to 58016 atoms, was minimised in order to remove bad contacts. This was followed by molecular dynamics simulations during which the temperature was progressively increased in 50-K steps to reach three different temperatures (310, 400, and 500 K; for MD simulation nomenclature see Table 1). Using different initial velocities, three and five independent simulations were performed at 400 and 500 K, respectively. Then, production runs were performed in the NPT ensemble and conformations were stored every 1 ps for further analysis.

The corresponding densities of water were 0.99 g cm^{-3} at 310 K, 0.89 g cm^{-3} at 400 K, and 0.71 g cm^{-3} at 500 K. These values for the water density are in the same range as the experimental values.

The Amber package was used for energy minimization and MD simulation. The Shake algorithm (Kräutler et al. 2001) was used to fix all bonds involving hydrogen atoms, which enabled the use of a 2-fs time step for integration of the equation of motion. The particle mesh Ewald summation (PME) (Essmann et al. 1995) was used for electrostatic interactions, and periodic boundary conditions were applied to avoid edge effects.

The molecular dynamics simulations used for refinement of the selected intermediates, made up to more than 115000 atoms, were performed under identical conditions.

All the simulations represent more than 130 ns of MD simulation in explicit water. All computations were performed on a multi-processor (Linux Beowulf clusters) with four dual 3.06 GHz Intel Xeon processors, and each nanosecond required approximately 2.5 days CPU time.

NMR experiments

The backbone resonances were assigned using standard triple-resonance techniques (Cavanagh et al. 1996) at 288 K and have been submitted to the BMRB (accession no. 16615; www.bmrb.wisc.edu). HNCACB and CBCA(CO)NH experiments were performed on a Bruker Avance 800-MHz spectrometer whereas HNCO, HNCA, and HN(CO)CA were performed on a Varian Unity Inova 600-MHz spectrometer.

To obtain qualitative information about the $N_2 \leftrightarrow I_2$ equilibrium, a series of ^{15}N HSQC spectra at different temperatures (288, 291, 294, 297, 300, 303, 306, and 309 K) were also recorded consecutively on the Varian spectrometer.

NMR relaxation experiments were performed on a ^{15}N-labeled sample of EcHUβ_2 (1.3 mM) at 288 K and 300 K on a Varian Inova 600-MHz (NOE, R_1, and R_2) spectrometer. ^{15}N T_1 and T_2 spectra were acquired with 32 scans per t1 point with a recycle delay of 3.0 s. T_1 relaxation delays of 10, 50, 100, 200, 300, 400, 500, 600, 700, 800, 900, 1000, 1250, and 1500 ms were used for data collection. T_2 relaxation delay times of 10, 30, 50, 70, 90, 110, 130, 150, 170, 190, 310, and 410 ms were used for data collection. The errors in R_1 and R_2 were determined by generating random distributions of the measured intensity within the $I \pm \Delta I$ range and by repeating the fit 1000 times with this procedure. The ^{15}N NOE spectra were collected with a 3 s presaturation period and a 3 s relaxation delay; the reference experiment had an equivalent 6 s delay. Both were acquired with 64 scans and were run twice under the same conditions. The ^{1}H–^{15}N NOE was obtained from the ratio of the peak intensities with and without the 3 s proton saturation. The NOE error was calculated using the signal-to-noise ratio. Hydrogen exchange protection factors were calculated as described by Arrington and Robertson (2000). All NMR data were processed with NMRPipe software (Delaglio et al. 1995) and chemical shift perturbations, intensity changes, and line widths of the peaks were analysed with Sparky (Goddard and Kneller 2001) and CcpNmr (Vranken et al. 2005).

Results

MD simulations

The N_2 to I_2 thermal transition of EcHUβ_2 was simulated by molecular dynamics (MD) simulations. We first performed a 310 K MD simulation without observing any significant structural change in the dimer, which remained native-like over 25 ns (MD_1^{310}, red curves, Fig. 1). This simulation was used as a control for the other MD

simulations. To accelerate the process, we performed high-temperature MD simulations at 400 and 500 K to access the N_2 to I_2 thermal transition in a time range attainable by MD simulation (Fig. 1a; Table 1). An overview of the simulations is given in the Supplementary material. At 500 K, the C^{α} RMSD rise was too rapid for any intermediate to be observed (MD_1^{500} to MD_5^{500}) and at 400 K, the thermal unfolding process was slower and less structurally destabilizing (MD_1^{400} to MD_3^{400}, Fig. 1a).

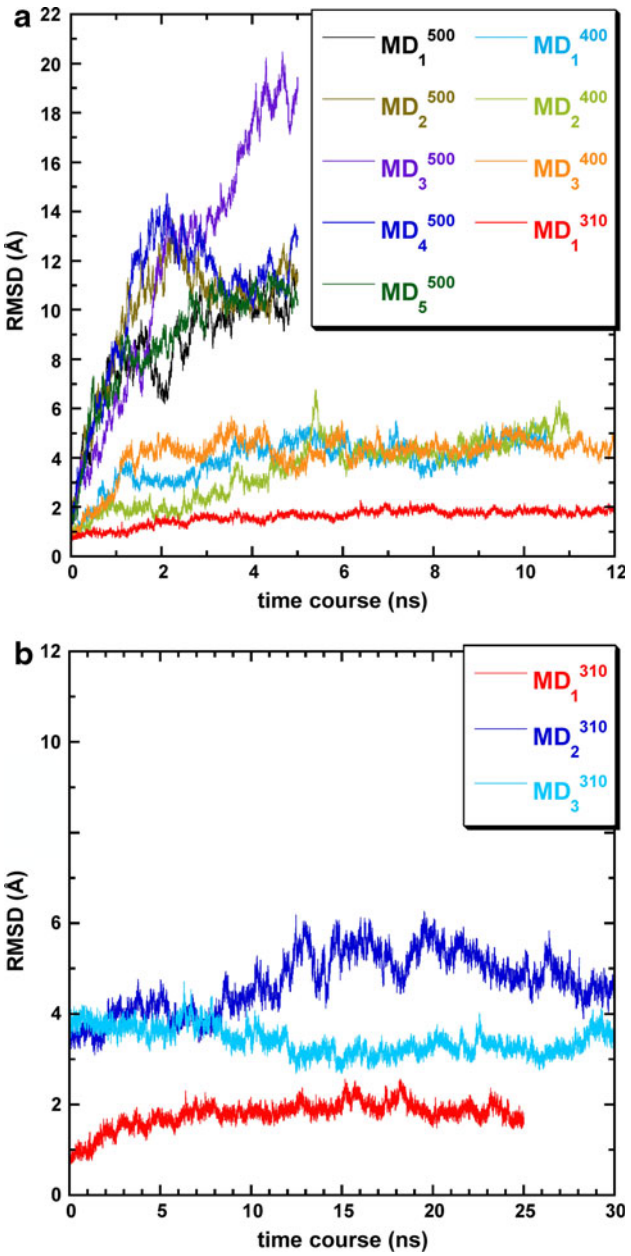

Fig. 1 MD simulations. **a** Root mean square deviations (RMSD) of C^{α} protein atoms from the EcHUβ_2 model at 310, 400, and 500 K as function of simulation time. **b** C^{α} RMSD during 310 K trajectories of the C_4 intermediate extracted from MD_1^{400} (MD_2^{310}) and MD_3^{400} (MD_3^{310}) and of the native state N_2 (MD_1^{310})

Identification in 400 K trajectories of a kinetic intermediate with secondary structure features similar to those of the experimental thermal intermediate, I_2

The 400 K simulations enabled us to examine whether a kinetic intermediate (i.e. a cluster of similar conformations, see Supplementary material Fig. 2S) identified along 400 K trajectories reproduced the experimental CD observations we made on the thermal intermediate I_2 of EcHUβ_2 (Ramstein et al. 2003). To screen the clusters of conformations during simulations, we considered only the mean value of the secondary structure content of these clusters as the main selection criterion. For each 400 K trajectory, we were thus able to identify at least one cluster of conformations with structures similar to the experimental secondary structures observed for I_2: C_4, C_8, and C_4 of MD_1^{400}, MD_2^{400}, and MD_3^{400}, respectively (italicised in Table 2). Although these clusters had global structural similarities, their mean structures were not completely superimposable. For instance, cluster C_4 of MD_1^{400} had approximately 10% more helical structures than I_2(exp) and C_4 of MD_3^{400} had approximately 10% more β-structures (Table 2). For both C_4 clusters, one of the $\alpha 2$ helix C-terminal cappings was alternately present or absent (fluctuation between 3 and 10 Å) on one protomer, resulting in a partial unfolding of the $\alpha 2$ helix from the middle of the helix to its C-terminal end and the frequent loss of the β structure nature of the two $\beta 1$ short strands (Fig. 1S).

Structural and dynamic behaviour of the dimeric intermediate extracted from MD simulations

Along 400 K trajectories, structural and conformational clustering analysis indicates that there is an early C_4 intermediate with conformations containing secondary structure elements similar to those estimated by CD experiments for the thermal intermediate I_2. To refine the 3D structure of this intermediate, we extracted from the C_4 clusters (in MD_1^{400} and MD_3^{400}) one conformation having secondary elements equal to those of the mean structure of the cluster and used it as the initial model to perform new MD simulations at 310 K (37°C) for 30 ns (Fig. 1b). This temperature was chosen because previous DSC experiments indicated that EcHUβ_2 preferentially adopts its I_2 conformation at 310 K (37°C) with an N_2 to I_2 thermal transition at 300 K (27°C). Because both C_4 intermediates (from $MD_1^{400}$and MD_3^{400}) converge to similar conformation sets (mostly for the protein body) during both independent 310 K trajectories (MD_2^{310} and MD_3^{310}, respectively), we described below a detailed analysis of the MD_2^{310} trajectory (Fig. 1b, dark blue curve). If the C_4 cluster corresponds to good conformational model sets for the intermediate I_2, it ought to be relatively stable at 310 K (37°C, the

Table 1 MD simulation nomenclature

Temperature (K)	Simulation name	MD duration (ns)
310	MD_1^{310}	1 × (25)
400	MD_1^{400}, MD_2^{400}, MD_3^{400}	3 × (10)
500	MD_1^{500}, MD_2^{500}, MD_3^{500}, MD_4^{500}, MD_5^{500}	5 × (5)
310	MD_2^{310} (for $C_4MD_1^{400}$)	30
(C_4 intermediate refinement, C_4^{ref})	MD_3^{310} (for $C_4MD_3^{400}$)	30
Total		140

physiological temperature for *E. coli*) as previously predicted (Ramstein et al. 2003). During simulation, the C^{α} RMSD fluctuated between two extreme values (4 and 6 Å, calculated in relation to the starting structure N_2). Similarly, the radius of gyration fluctuated between 14.8 and 15.8 Å and can be associated with a slight breathing of the dimer intermediate (as compared with 14.2 ± 0.2 Å of the native structure "N_2" at 310 K; Fig. 1b, red curve). A global inspection of the conformations generated indicates that the C^{α} RMSD bulge from 4 to 6 Å (absent in MD_3^{310}) rests on structural rearrangements of the very flexible protein arms rather than on drastic structural remodelling in the protein body between the two 310 K simulations. The C_4 conformations of both 310 K trajectories correspond to dimer molecules having lost numerous native secondary structures (Fig. 2):

1 the α-helical structure of the *α3* helix at the C-terminal end of both protomers (residues K83–N90);
2 approximately 30–40% of the native α-helical structure of both the two *α2* helices (C-terminal part: residues A27–K37); and
3 1 to 5% of the *α1* helices (N-terminal part: residues N2–Q5) during the last 7 ns.

On the other hand, the *β*-strands of both *β*-sheets were still present after 24 ns (*β2* and *β3*). Interestingly, at the beginning of the 310 K simulation (i.e., until 8–10 ns), the native secondary structure contents were significantly different on both subunits, despite the twofold symmetry axis between both protomers in the native dimer body (Fig. 1Sc). Except for the short strand *β1*, they tended to be relatively similar in both subunits in the last 14 ns, even if the twofold symmetry axis is lost (Fig. 2). If we do not take into account the structural dynamics of the dimer arms (residues 55–75), overall similar observations can be made for both independent 310 K simulations (MD_2^{310}, MD_3^{310}). In the case of $C_4(MD_3^{400})$, both arms of the thermal intermediate remained native-like during the 30 ns of the

Table 2 Secondary structure content of identified conformation clusters in 400 K simulations

Cluster	Remaining secondary structure content (%)						SASA (Å^2)		
	α-structures			β-structures					
	MD_1^{400}	MD_2^{400}	MD_3^{400}	MD_1^{400}	MD_2^{400}	MD_3^{400}	MD_1^{400}	MD_2^{400}	MD_3^{400}
C_1	88	85	85	94	95	92	8063	7914	8099
C_2	83	84	69	84	95	92	8356	8230	8575
C_3	71	87	67	76	92	94	8341	8033	8504
C_4	*68*	90	*60*	*79*	101	*86*	*8327*	8063	*8342*
C_5	77	75	63	80	96	87	8476	8337	8480
C_6	67	75	51	62	102	80	8293	8420	8294
C_7	69	78		54	73		8370	8239	
C_8	75	*69*		47	*74*		8386	*8330*	
C_9	86			47			8506		
C_{10}	79			28			8378		
I_2 (exp)		59			78		–	–	–
C_4^{ref}									
MD_1^{400}		62			60		7460		
MD_3^{400}		57			80				7908

The remaining secondary structure content is expressed as a percentage of that of the native state N_2 used as the MD starting model (see also "Materials and methods" section). The nomenclature of simulations is given in Table 1. I_2(exp) refers to the thermal intermediate identified by DSC experiments for which secondary structure content was determined from CD spectra at 10°C (310 K) over the melting temperature of the first transition (Tm = 27°C, i.e. 300 K) and normalised in relation to N_2 (Ramstein et al. 2003). *Italics* indicate clusters of conformations with a secondary structure content proximate to that of I_2(exp) in each 400 K simulation. C_4^{ref} corresponds to a mean structure of C_4 conformations calculated from C_4 conformations generated during the last 10 ns of the 310 K simulations MD_2^{310} and MD_3^{310}. SASA is solvent-accessible surface area

trajectory (data not shown), explaining the differences between the remaining β-structures with regard to the conformations generated from both initial C_4 and the lower RMSD observed in the MD_3^{310} simulation (Table 2; Fig. 1b).

In the last 10 ns of both 310 K trajectories (MD_2^{310} and MD_3^{310}), the protein conformations generated were very close (on average, 0.8 Å for C^{α} RMSD between them considering only the protein body), which testifies to the stability of the thermal intermediate at 310 K, as expected from previous experiments. The structural transition between the initial model "N_2" and the C_4 intermediate was clearly associated with the loss of quaternary and tertiary structures involved in the dimer stability. Thus, the loss of the *β1* strand and the drastic remodelling of the C-terminal part of helices *α2* depend on the break of the intra-subunit salt bridges S35-D40 (the C-terminal capping of helix *α2*, Figs. 1Sa, 3Sa) and on the unfolding of helix *α3* initially stacked by its N-terminus on the C-terminal part of helix *α2* (see the structure of the native dimer, Fig. 1Sc). The continuity of helix *α2* was interrupted early by a kink centred on residues A30–V32 of both large helices *α2* whose C-terminal ends (from A27 to K37) were partially unfolded (Fig. 2). From NMR experiments, the discontinuity of *α2* occurring at around residues V32–T33 was also demonstrated for EcHUβ_2 at 288 K, suggesting an intrinsic instability of this large helix (see below). Interestingly, the stability of the N-terminal part of helix *α2* was associated with the intermolecular coiled-coil interaction A24–A24′ (one of the strong quaternary interactions implied in the stability of the dimer; Figs. 1Sc, 3Sb). On the other end, the central part of the helix *α1* (Q5–I10) remained highly stable throughout 310 K simulations and its relative orientation with the remaining native-like part of the helix *α2* was relatively conserved while the relative orientation between both HTH motifs was significantly modified. The apparent stability of helix *α1* correlates with the apparent rigidity of turn 1 (T1, Fig. 1S) (Kawamura et al. 1996) which contains the N-terminal capping of helix *α2* (the hydrogen bond S17–A19; Fig. 3Sc) and the C-terminal capping of the helix *α1* (the intra-subunit salt bridges D8–K18; Fig. 1Sb). Although the S17–A19 intra-protomer link endured during 310 K simulations, the D8–K18 interaction was alternately interrupted (Fig. 3Sc, d, respectively). Only a short N-terminal part of helix *α1* (residues M1–S4) was slightly unfolded (Fig. 2), dynamic behaviour which might be related to its N-terminal position and to the alternate loss of the inter-subunit salt bridges M1–D40′ and M1′–D40, one *β1* strand, and both C-terminal parts of helices *α2* (Figs. 1Sc, 3Se). Concerning the tertiary fold, the α1–α2 crossing angle of the remaining part of the HTH motif slightly increased on average from 102.8 ± 5.0° in the native structure (N_2, at 310 K) to 109.0 ± 5.0° in the C_4 intermediate (Fig. 3Sf). At the same

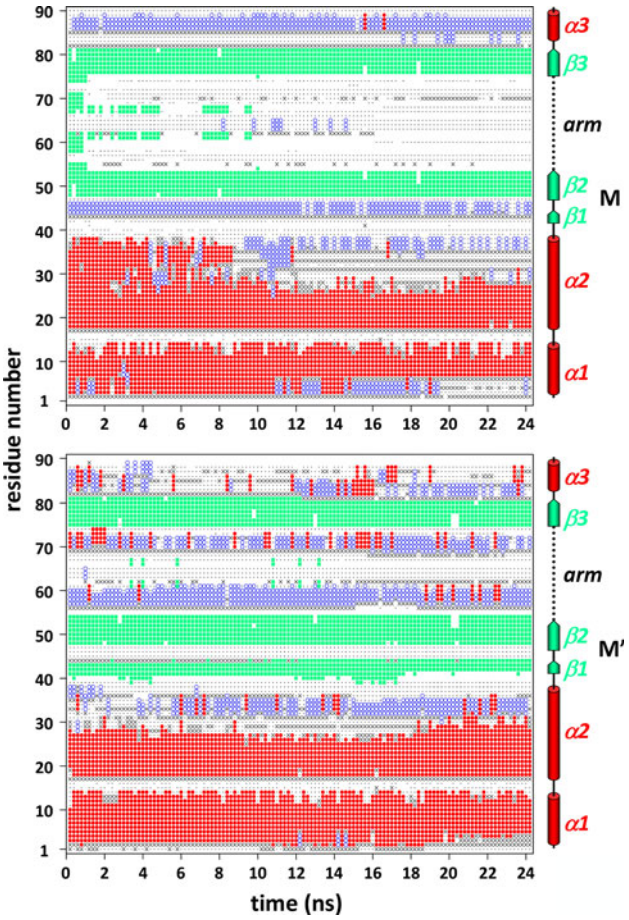

Fig. 2 Time course of the secondary structure of the $C_4(MD_1^{400})$ intermediate for the 310 K simulation MD_2^{310}. Secondary structures were assigned according to MOLMOL (Koradi et al. 1996): *filled red circle*, α-helix; *open blue circle*, 3_{10}-helix and π–helix; *filled green square*, β-strand; *black cross*, turn; *point*, β-bridge or bend structures; *no symbol*, other and random structures. *M* and *M′* are for protomers 1 and 2, respectively

time, the pseudo-continuity between both β-sheets of the dimer was maintained by inter-subunit contacts between both *β3* strands, thus preserving the compact structure of the hydrophobic core of the dimer. Although the twofold symmetry axis was partly conserved between both subunits at the level of the hydrophobic core (β-strand-rich subdomain of the body), it was lost between the two remaining HTH motifs (α-helix rich subdomain of the body). Except for the pseudo-symmetric unfolding adjustment of helices *α2*, the thermal intermediate C_4 identified in 400 K simulations was stable throughout 310 K simulations and corresponds to a dimer having essentially lost native α-helical structures.

NMR experiments

Nuclear magnetic resonance (NMR) is not only a technique to obtain protein structure but is also particularly convenient for monitoring, at the atomic level, structural and/or

environmental changes. In particular, heteronuclear shift correlation experiments, for example ^{1}H–^{15}N HSQC, are very useful for detecting alterations in the electronic environment of atoms which affect their chemical shifts. Conformational change necessarily involves the exchange of the nuclei or molecules being observed between at least two states—N_2 and I_2 states in our case. The effect of this exchange process on the appearance and the interpretation of the NMR spectrum, for example HSQC, depends on the k_{ex} value. When the exchange is very slow on the "NMR timescale", here relative to the magnitude of the chemical shift difference between the two states, two separate resonances are found at the positions corresponding to the chemical shifts characteristic of the two states, but their relative intensities will depend on their relative populations (Durney et al. 2004). If the exchange is very fast relative to the chemical shift difference, a single resonance is observed whose position is the average of the chemical shifts of the two states, weighted by their relative populations (the easiest regime for interpretation of the spectra). Between these extremes there are complex changes in line shape which result in the observation of very broad low-intensity signals. Hence, analysing the intensity differences and the line-broadening evolution of the HSQC peaks can provide preliminary insights into the dynamics of the protein.

At 288 K, the ^{15}N HSQC spectrum of EcHUβ_2 was well dispersed—confirming that the protein is folded—and is typical of an $(\alpha + \beta)$ homodimer protein (90 peaks expected instead of 180) containing solvent-exposed α-helices (poorly resolved peaks at 8 ppm) and β sheets (peaks downfield to 9 ppm). The backbone sequential assignment of the EcHUβ_2 NMR spectra was successfully achieved as described in the "Materials and methods" section (89% of non-proline residues) and was deposited in the BMRB (accession number 16615). Assignment of the side-chains and determination of the 3D NMR structure of the protein is still in progress, but preliminary results can be obtained from the backbone chemical shifts analysis. As Wishart and Sykes demonstrated, the chemical shifts, in particular C^{α}, are statistically correlated with the local backbone conformation and can therefore be used as secondary structure predictors (Wishart et al. 1995; Wishart and Sykes 1994). The secondary structure elements predicted by the CSI program are given in Fig. 1Sa and are compatible with those derived from the model N_2. The main discrepancies are that α_1 is predicted to be shorter (which can be explained by a lack of NMR data) and that α_2 seems to be kinked at residues 32–33. The chemical shifts can also be used to provide estimates of the Φ and Ψ angles, an idea that has been implemented in TALOS software for the prediction of backbone torsion angles using H^{α}, C^{α}, C^{β}, C', and N chemical shifts (in our case H^{α} was not used) and the primary protein sequence (Cornilescu et al. 1999). TALOS could not predict Met1 and Asn90 because of their position in the sequence and S4, Q5, and D26 because of a lack of NMR data. Seven residues (T33, V45, G46, A57, G60, A73, and A74) were classified as ambiguous by the software and only two (D15 and G48) were classified as bad, so almost 85% of the residues were classified as good. Because Ψ is a much more discriminating indicator than Φ of the main favoured regions in the Ramachandran plot, we compared the TALOS predicted Ψ angles with those derived from the N_2 models of the protein: only three residues (V32, T33, F47) had a significantly different Ψ angle value in the TALOS prediction. In summary, it can be concluded from the CSI and TALOS predictions that our preliminary NMR data are in agreement with the N_2 model with indications that the $\alpha 2$ helix (Residues 18–38) could exhibit dynamics or could be kinked in solution.

Because previous experiments have shown that HU dimers undergo a three-state thermal unfolding process involving a dimeric intermediate species ($N_2 \leftrightarrow I_2 \leftrightarrow 2D$), ^{15}N HSQC experiments at different temperatures (Fig. 3) were used to follow the H^N chemical shifts and the intensity of all the NHs during the first thermal transition ($N_2 \leftrightarrow I_2$) which should occur at approximately 300 K and thus determine the protein secondary element relative stability and/or structural changes.

If one assumes that increasing temperature does not produce any major structural changes in the protein but leads to an increase in the local thermal fluctuations, then one can predict that it would cause chemical shifts to move

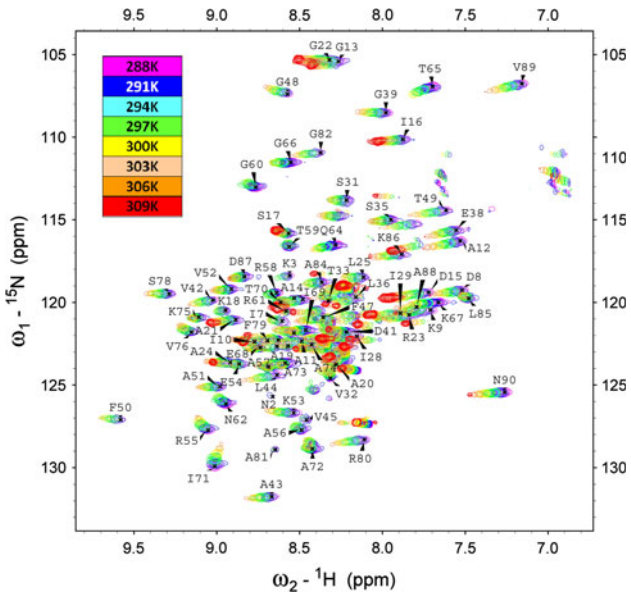

Fig. 3 Overlap of 2D ^{1}H–^{15}N HSQC spectra of EcHUβ_2 at different temperatures

towards their random-coil positions. These temperature-dependent changes in chemical shift are generally linear up to approximately 288 K (15°C) below the global denaturation temperature (Baxter and Williamson 1997). When the temperature was gradually increased (3 K/step), neither large variations in chemical shifts nor collapsing of chemical shifts (no denaturation process) were observed over the temperature range used (294–309 K) (Fig. 3). For most H^N chemical shifts the temperature dependence was linear. For more than 20% of the protons, however, a curved temperature dependence was observed, indicating that at least two species of the protein were in fast exchange over the temperature range studied (data not shown). These results were confirmed by preliminary dynamics study of the protein, by looking at the peak intensities. Indeed, peak intensity is correlated with the transverse relaxation time T_2: an increase in internal dynamics can be observed if peak intensities decrease (Cavanagh et al. 1996). While temperature increased, peak intensities globally decreased and only a few signals (around 8 ppm) were still observed at 309 K (36°C). The disappearance of NMR peaks results from an increase in global dynamics (tumbling time of the protein), an increase in internal dynamics on the microsecond to millisecond time-scale, and on exchange phenomena. In our case, solvent exchange is too fast (see text below and Fig. 5S) to be the main cause of the disappearance of the peaks. In order to eliminate the global dynamics dependence, all the NH intensities were normalised with those of seven residues which did not undergo any change (within measurement error) when temperature increased. Figure 4a shows the normalised intensity (I_N) profile of the protein at 298 K. As shown in previous NMR studies on the HU homodimer from *B. subtilis* and *B. stearothermophilus*, the arm (56–73) is the most dynamic part of the protein even at low temperature (Raves et al. 2001; Vis et al. 1995).

In order to compare the evolution for all amino acids, relative intensity ratios ($I_R = I_N/I_{288K}$) of each NH backbone were calculated. An overview of the temperature-dependence of these ratios is shown in Fig. 4 (see also Fig. 4S). On the basis of the evolution of the relative intensity, the protein residues can be sorted into three classes. Residues 13–14, 16–17, and 20–22 belong to the first class and correspond to the central part of the HTH motif. Their intensity ratios are not affected by heating, leading us to propose that the most stable domain of EcHUβ_2 is the central part of the HTH motif, as suggested by MD simulations. The second class includes residues 8–12, 15, 23–32, 35, 38–44, 47–53, 55, 71, 74–78, 80, 82, and 85–90. Their intensity ratios were stable up to approximately 300 K and then decreased linearly with temperature (Fig. 4b). It is important to note that all these residues are located in both α helices and β strands. This tendency seems to prove that the protein undergoes local structural changes and a sudden dynamics increase at approximately 300 K (which corresponds to the melting temperature of the first thermal transition) (Ramstein et al. 2003). For example, residues 23–32, 35, and 38 are located in the $\alpha 2$ helix, which is thought to be partially unfolded in the I_2 model. In the third class we found residues 3, 7, 18–19, 45, 54, 56–70, 72–73, 81, and 84. Their intensity ratios decreased almost linearly and rapidly with temperature (Fig. 4c). These residues are in flexible regions of the protein even at low temperature, reflecting the fact that they already have multiple possible local conformations. The temperature dependence of their intensities is then linked to an increase in their dynamics.

NMR relaxation experiments (R_1, R_2, and NOE) were performed at 288 K (Fig. 4d–f) and 300 K (data not shown) in order to investigate more accurately the internal dynamics of EcHUβ_2. The dynamics of EcHUβ_2 were highly similar to those observed for HUB*st* (Vis et al. 1995): the general pattern observed in the relaxation data at both temperatures is that the residues of the arm are more flexible than those in the rest of the protein. Lower values for transverse relaxation rates and for the ^{15}N heteronuclear NOE compared with the core of the protein indicate enhanced mobility. Interestingly, three residues V32, T33, and F79 had R_1, R_2, and NOE values close to those of the residues belonging to the arm at 288 K. The mobility of V32 and T33 confirmed that the $\alpha 2$ helix (residues K18–K37) had a dynamic kink centred on these residues.

HSQC-based amide exchange experiments were performed at 288 K. On the first point (20 min), only 15 peaks remained, indicating that approximately 80% of the residues of the protein underwent fast exchange with the solvent. Complete exchange (no observable signal) was achieved after 2 h. The protection factor calculated from amide proton exchange (Fig. 5S) indicates that the central part of the HTH domain is more stable than the other part of the protein. This solvent accessibility of the HTH motif also fits well with the Lon proteolytic sites in EcHUβ_2 (Liao et al. 2010).

The results from the NMR study are in agreement with the I_2 model proposed by MD simulation. NMR structure determination at 288 K (15°C) and 300 K (27°C) is in progress. Nevertheless, obtaining enough data at 300 K (27°C) to be able to produce a high-resolution 3D structure is still a challenge because of the small intensities of the peaks.

Discussion

To simplify comparison between N_2 and C_4 (a possible model for I_2), we calculated a mean 3D structure from

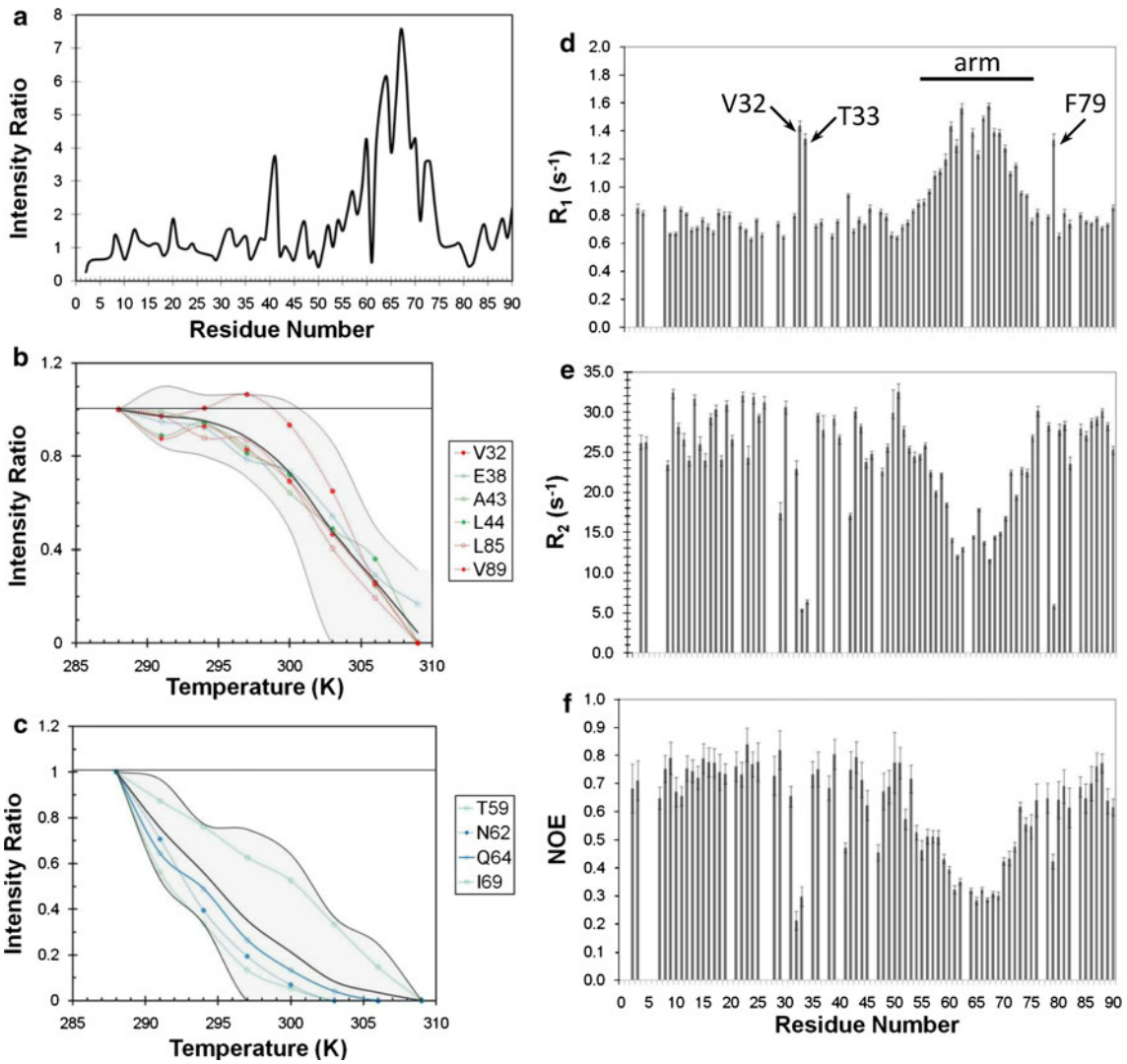

Fig. 4 NMR dynamics study of EcHUβ_2 **a** Normalised intensity profile at 288 K of the HSQC peaks. (**b**, **c**) Temperature-dependence of the relative intensity of HSQC peaks for a set of residues belonging to secondary structure elements in the N_2 model (**b**) and to very flexible parts (**c**): α-helix residues are shown in *red*, *β*-strand residues in *green*, and residues which are neither in α-helices nor in *β*-strands are shown in *light blue*. The *bold black curve* represents the average intensity ratio for all the residues having the same dependence. *Black curves* correspond to the minimum and maximum ratios observed. More details can be found in Fig. 4S. **d**–**f** R_1, R_2 and NOE at 288 K. Lower values of R_2 and NOE indicate increased flexibility on a ps–ns timescale

conformations generated during the last 10 ns, called C_4^{ref} (for "refined structure of C_4" at 310 K, Table 2). As both C_4^{ref} (extracted from MD_2^{310} and MD_3^{310}) are very similar (C^{α} RMSD of 0.9 Å), the structural model extracted from MD_2^{310} will be mainly discussed below.

The overall electrostatic and topological surface of C_4^{ref} is significantly remodelled as compared with the native structure N_2 of the homodimer (Fig. 5). Despite its overall compact structure, C_4^{ref} displays numerous residues, initially buried in the hydrophobic core of the protein (mostly belonging to helix *α2* and to the *β1* strand: I29, V32, L36, V42, A43, L44, I71, P77, and F79) and now exposed to solvent molecules. The protein body collapses slightly at the interface between the α-helix-rich subdomain and the *β*-strand-rich subdomain (Fig. 6). This is associated with significant changes in the relative orientation and interaction between both subdomains in the dimer body and between protomers at the HTH level. The surface area of the protein contains numerous small crevasses and a tunnel which perforates the protein body from one side to the other. The very large protein pocket of the intermediate results from opening of the large interfacial cavity (area 246.5 $Å^2$) of the EcHUβ_2 body (Fig. 6Sa). In its N_2 state, the interfacial cavity of the dimer is essentially covered, at the bottom by the residue side chains of the central and C-terminal parts of the large *α2* helix (L25, I28, I29, and

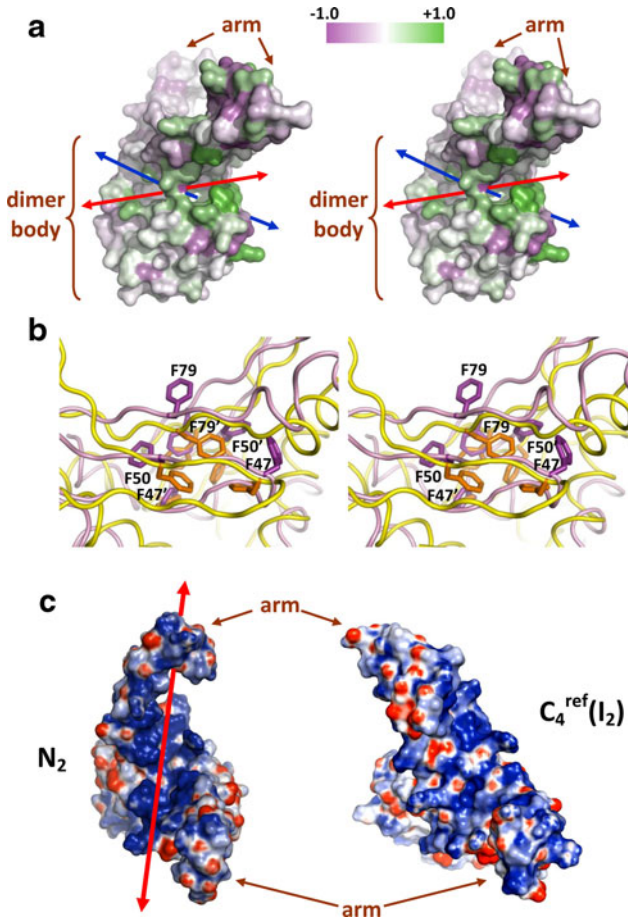

Fig. 5 Quaternary fold of the C_4 refined structure, C_4^{ref}, at 310 K **a** Stereoviews of the solvent-accessible surface area (*SASA*). The *colour code* of the area indicates differences in SASA for each residue between the native EcHUβ_2 and C_4^{ref} in relation to the sum of SASAs (a gradation in colour from *magenta* to *green* indicating more buried to more exposed residue in C_4^{ref}, the *white area* indicating no change in SASA between both structures). *Red* and *blue arrows* indicate protein body perforations. **b** Superimposition of the aromatic clusters of the native EcHUβ_2 and C_4^{ref}. The minimised starting model for MD simulation of EcHUβ_2 and C_4^{ref} are shown in *yellow* and *magenta*, respectively. **c** Comparison of the charge distributions at the protein surface between EcHUβ_2 (N_2) and the simulated thermal intermediate C_4^{ref} (I_2). *Blue regions* indicate basic surfaces and *red* and *white* regions indicate acidic and neutral surfaces, respectively

V32 of both chains) and at the top by the inner surface of the β-sheet subdomain (L44 of the *β1*strand, F47 of turn *T3*, and F50 of the *β2* strand of both chains). In C_4^{ref}, I29 and V32, are now exposed to solvent molecules. The transition from an interfacial cavity (in N_2) to a large pocket (in C_4^{ref}) mainly correlates with the structural remodelling of the C-terminal part of the *α2* helices (residues D26–E38) coupled with a slight change in the β-sheet domain (essentially the *β1* strands, A43–V45), the *T2* turns (residues G39–V42), and of the loss of the *α3* helices (residues K82–N90) (Fig. 2). Through 310 K trajectories, and as expected, the secondary structure contents of the HTH motif of C_4^{ref} remain consistent with previous CD experiments (Table 2) (Ramstein et al. 2003). On the whole, the structural description of the I_2 (C_4^{ref}) state of EcHUβ_2 is also in agreement with the NMR experiments presented above. This is particularly true for the HTH motif displaying structural changes in the C-terminal parts of helix *α2* (A27 to K37 associated with the atypical dynamics behaviour of V32 and T33 at 288 K, Fig. 4) when the central part of the HTH motif appears more rigid, as also predicted by NMR experiments (Fig. 4 and Fig. 4S).

In C_4^{ref}, the protomer interface area remains similar to the native conformation of the dimer (approx. 2000 Å^2, the loss of native contacts being compensated for by new hydrophobic collapses). The large cavities found in *E. coli* HU dimers (particularly in EcHUβ_2) are a weak point of the dimer structure, probably associated with the thermal N_2 to I_2 transition, as has previously been proposed for other oligomeric proteins (Bueno et al. 2006; Sonavane and Chakrabarti 2008). This proposition is supported by the experimental observation that the HU homodimers so far studied (BstHU and BsuHU, HUs from *B. stearothermophilus* and *B. subtilis*, respectively) display a two-state thermal unfolding process without passing through a dimeric intermediate (Ramstein et al. 2003). Thus, the interfacial cavity of BstHU is partially filled in by two additional phenylalanines at position 29 in the *α2* helix (White et al. 1999). This stabilises the large *α2* helices, by significantly reducing the interfacial cavity area (51.6 Å^2) compared to *E. coli* HU dimers (Fig. 6S). This enables the aromatic cluster to extend from the β-strand-rich subdomain to the buried part of the HTH motif, thus strongly associating the two subdomains of these dimers (creating additional aromatic interactions between F29 of both the *α2* helices and the six other phenylalanines contained in the β-strand-rich subdomain). These additional interactions make a major contribution to the thermal stability of the dimer and may stabilise the HTH motif of BstHU and BsuHU (F at position 29 is conserved in both dimers, Fig. 6Sc). In the latter cases, the HU body has been described as a single-energy domain, in contrast with *E. coli* dimers (Kawamura et al. 1996, 1997; Ramstein et al. 2003; Ruiz-Sanz et al. 2004; Welfle et al. 1993). Accordingly, we propose that the three-state thermal unfolding process ($N_2 \leftrightarrow I_2 \leftrightarrow 2D$) of the *E. coli* HU dimers is connected, in part, to the presence of a large interfacial cavity and to the absence of F29. However, an F residue at position 29 is not an absolute criterion, because the HU protein from the hyperthermophile *Thermotoga maritime* (TmHU) has a Leu residue at this position and follows a two-state unfolding process ($N_2 \leftrightarrow I_2$) (Esser et al. 1999; Ruiz-Sanz et al. 2004). Despite the absence of an additional F residue, the NMR study revealed that TmHU has a small interfacial

cavity (of approx. 50 Å^2) similar to that of BstHU (Durney et al. 2004). This study also showed that TmHU can exist in two states: a rigid major form close to the HU X-ray structures and a very flexible minor form mainly affected in its α-helical elements. As already suggested, this structural and dynamics observation implies similarity between hyperthermophilic (TmHU) and mesophilic (EcHU) proteins. The high deuterium exchange rates of BstHU helical elements determined by Raman spectroscopy are also supportive of intrinsic flexibility at the dimeric interface which we suggest is exacerbated in EcHUβ_2 (Serban et al. 2003).

In C_4^{ref}, the aromatic cluster and β-sheets are still present but, though buried (except F79 of one protomer), the native orientations of the phenylalanine side chains are significantly changed and their relative orientations fluctuate during the 310 K simulation (Fig. 5b). This dynamic behaviour correlates with relaxation measurements and Overhauser enhancement data showing the atypical behaviour of F79 (Fig. 4). The concave surface defined by the saddle-like β-sheet structure of both subunits is significantly affected whereas the native β-sheet structure of each protomer and the twofold symmetry axis are locally maintained. As for N_2, the dimeric nature of C_4^{ref} is also stabilised by regular maintenance of at least one of the interchain salt bridges M1–D′40 and M1′–D40 (Fig. 3Sd). In this way, the dimeric nature of C_4^{ref} essentially rests on the aromatic core and on the central part of the HTH motif via the coiled-coil interaction A24–A24′ (Fig. 1Sc).

The saddle-like β-sheet structure in N_2 defines a very basic surface which is neutralised by DNA through binding (Swinger et al. 2003). In C_4^{ref}, this basic groove is completely lost (Fig. 5c), suggesting that the thermal intermediate we identified by simulations might be affected in DNA recognition. This is in good agreement with our observation that the I_2 thermal intermediate of EcHUβ_2 is unable to bind specifically to single-stranded break-containing DNA (Ramstein et al. 2003).

The structural remodelling of EcHUβ_2 in C_4^{ref}, possibly associated with its transition to the I_2 conformation, might also provide a structural explanation for the Lon hypersensitivity of EcHUβ_2 (Bonnefoy et al. 1989; Liao et al. 2010). The recognition of a protein and its subsequent degradation by Lon might result from exposure of hydrophobic patches or structural motifs that are normally hidden in the core of the target protein (Tsilibaris et al. 2006). Interestingly, most of the preferred cleavage sites of Lon in EcHUβ_2 (Liao et al. 2010) are hyper-exposed to solvent molecules in C_4^{ref} as compared to their accessibility in the N_2 state (Fig. 6). This correlates with the observation that, in a *hupA E. coli* strain (devoid of EcHUα_2) in which *hupB* was over expressed, EcHUβ_2 does not accumulate in bacteria at 37°C (310 K) (Bonnefoy et al. 1989; Claret and Rouviere-Yaniv 1997). In the wild-type *E. coli* strain, EcHUβ_2 (produced at the end of the exponential phase) is protected from Lon degradation by recombining with EcHUα_2 in the heterodimer EcHU$\alpha\beta$ which is required for survival in the stationary phase. This former observation suggests that the physiological conformation of EcHUβ_2 is significantly different from those of the other *E. coli* HU dimers which are resistant to the Lon protease at 37°C (Liao et al. 2010). Thus, the physiological N_2 to I_2 conformational transition of EcHUβ_2 can be regarded as a molecular mechanism found by bacteria to maintain a free protein pool not engaged in DNA interactions and, therefore, available to produce heterodimer under physiological conditions (see below). In contrast, EcHUβ_2 accumulates during *E. coli* cold-shock adaptation suggesting that the conformational equilibrium is displaced from I_2 to N_2 and consequently, EcHUβ_2 becomes Lon-resistant (Giangrossi et al. 2002; Gualerzi et al. 2003). Combining all these observations, an I_2 conformation with a similar 3D structure to C_4^{ref} is in agreement with EcHUβ_2 Lon hypersensitivity.

The open structure we described for I_2 can also provide an explanation of the propensity of EcHUβ_2 to oligomerise at room temperature (Rouviere-Yaniv and Kjeldgaard 1979).

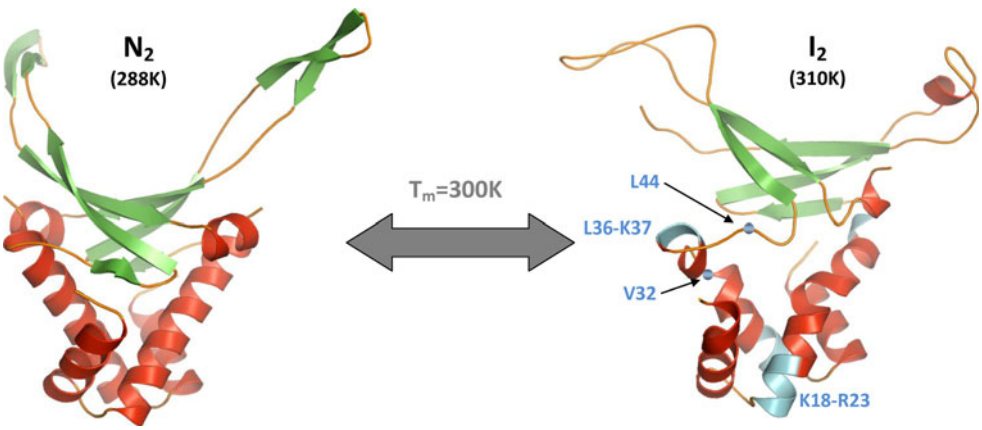

Fig. 6 Proposed structural model for the N_2 to I_2 transition of EcHUβ_2. *Blue* peptides and residue *balls* indicate the preferred Lon cleavage sites at 37°C (Liao et al. 2010) which are more accessible to solvent molecules in the I_2 model than in N_2. The *T*m value indicated for the transition was determined previously by DSC and was in agreement with this preliminary NMR experiment

Indeed in our model (Fig. 6), EcHUβ_2 exposes new structural determinants initially buried in its N_2 compact structure which can promote specific interdimeric interactions for the formation of tetramers and high-order polymeric structures (Fig. 7S and 8S). A similar control of the in-vivo protein oligomerization in response to environmental conditions has been described for the *E. coli* nucleoid protein H-NS (dissociation of an active homotetramer into inactive homodimers) (Stella et al. 2006). High-order oligomers of EcHUβ_2 might be useful during *E. coli* cold-shock adaptation. Along similar lines, we also propose that the I_2 conformations of *E. coli* HU homodimers are required for the formation of the heterodimer through a hetero-tetramer in which both homodimers exchange α and β subunits interacting by partial unfolding of their α-helix-rich subdomains (Fig. 8S).

During the past decade, high-temperature MD simulations have been extensively used to investigate the structural and dynamic behaviour of biological macromolecules (Armen and Daggett 2005; Rizzuti et al. 2004; Song et al. 2007; Wilson et al. 1990). Here, we used this strategy, combined with NMR experiments, to propose a structural model for the physiological dimeric intermediate I_2 of EcHUβ_2 (Fig. 6) that we had previously identified. Considering energetic (DSC), structural (NMR and CD), and functional studies (DNA binding and dimer oligomerization, this work, and Ramstein et al. (2003) and Rouviere-Yaniv and Kjeldgaard (1979)), C_4^{ref} extracted from simulations is the first realistic 3D model for the I_2 intermediate. Finally, we propose that the intrinsic instability of the $\alpha 2$ helix due to the high dynamics of V32–T33 (suggested by MD simulations and by NMR experiments) and the large interfacial cavity constitute the Achilles' heel of EcHUβ_2. We are now conducting new structural (MD, 3D NMR, and SAXS) and functional (heterodimer formation and site-directed mutagenesis) experiments with *E. coli* and other HU dimers to improve our model.

Acknowledgments This work was supported by the Centre national de la recherche scientifique (CNRS, France), the Ligue contre le cancer (Comités du Loiret, du Cher et de l'Indre, France), the Association pour la recherche contre le cancer (ARC, France), and by Electricité de France (EDF). We are greatly indebted to Nicolas Birlirakis (Plateforme technologique Nationale, ICSN, Gif-sur-Yvette, France) and Hervé Meudal, for their help in NMR data collection, and to Françoise Culard and Céline Landon, for critical discussion.

References

Armen RS, Daggett V (2005) Characterization of two distinct beta2-microglobulin unfolding intermediates that may lead to amyloid fibrils of different morphology. Biochemistry 44:16098–16107

Arrington CB, Robertson AD (2000) Kinetics and thermodynamics of conformational equilibria in native proteins by hydrogen exchange. Methods Enzymol 323:104–124

Baxter NJ, Williamson MP (1997) Temperature dependence of 1H chemical shifts in proteins. J Biomol NMR 9:359–369

Bonnefoy E, Almeida A, Rouviere-Yaniv J (1989) Lon-dependent regulation of the DNA binding protein HU in *Escherichia coli*. Proc Natl Acad Sci USA 86:7691–7695

Bonnefoy E, Takahashi M, Yaniv JR (1994) DNA-binding parameters of the HU protein of *Escherichia coli* to cruciform DNA. J Mol Biol 242:116–129

Boubrik F, Rouviere-Yaniv J (1995) Increased sensitivity to gamma irradiation in bacteria lacking protein HU. Proc Natl Acad Sci USA 92:3958–3962

Bueno M, Cremades N, Neira JL, Sancho J (2006) Filling small, empty protein cavities: structural and energetic consequences. J Mol Biol 358:701–712

Castaing B, Zelwer C, Laval J, Boiteux S (1995) HU protein of *Escherichia coli* binds specifically to DNA that contains single-strand breaks or gaps. J Biol Chem 270:10291–10296

Cavanagh J, Fairbrother WJ, Palmer III AG, Skelton NJ (1996) Protein NMR spectroscopy: principles and practice, 2nd edn. Elsevier Academic Press, USA

Claret L, Rouviere-Yaniv J (1996) Regulation of HU alpha and HU beta by CRP and FIS in *Escherichia coli*. J Mol Biol 263: 126–139

Claret L, Rouviere-Yaniv J (1997) Variation in HU composition during growth of *Escherichia coli*: the heterodimer is required for long term survival. J Mol Biol 273:93–104

Cornilescu G, Frank Delaglio F, Bax A (1999) Protein backbone angle restraints from searching a database for chemical shift and sequence homology. J Biomol NMR 13:289–302

Coste F, Hervouet N, Oberto J, Zelwer C, Castaing B (1999) Crystallization and preliminary X-ray diffraction analysis of the homodimeric form alpha2 of the HU protein from *Escherichia coli*. Acta Crystallogr D Biol Crystallogr 55:1952–1954

Delaglio F, Grzesiek S, Vuister GW, Zhu G, Pfeifer J, Bax A (1995) NMRPipe: a multidimensional spectral processing system based on UNIX pipes. J Biomol NMR 6:277–293

Durney MA, Wechselberger RW, Kalodimos CG, Kaptein R, Vorgias CE, Boelens R (2004) An alternate conformation of the hyperthermostable HU protein from *Thermotoga maritima* has unexpectedly high flexibility. FEBS Lett 563:49–54

Echols H (1990) Nucleoprotein structures initiating DNA replication, transcription, and site-specific recombination. J Biol Chem 265:14697–14700

Esser D, Rudolph R, Jaenicke R, Bohm G (1999) The HU protein from *Thermotoga maritima*: recombinant expression, purification and physicochemical characterization of an extremely hyperthermophilic DNA-binding protein. J Mol Biol 291: 1135–1146

Essmann U, Perera L, Berkowitz ML, Darden T, Lee H, Pedersen LG (1995) A smooth particle mesh Ewald method. J Chem Phys 103:8577–8593

Giangrossi M, Giuliodori AM, Gualerzi CO, Pon CL (2002) Selective expression of the beta-subunit of nucleoid-associated protein HU during cold shock in *Escherichia coli*. Mol Microbiol 44:205–216

Goddard TD, Kneller DG (2001) Sparky 3 NMR software, University of California, San Francisco

Gualerzi CO, Giuliodori AM, Pon CL (2003) Transcriptional and post-transcriptional control of cold-shock genes. J Mol Biol 331:527–539

Kawamura S, Kakuta Y, Tanaka I, Hikichi K, Kuhara S, Yamasaki N, Kimura M (1996) Glycine-15 in the bend between two alpha-helices

can explain the thermostability of DNA binding protein HU from *Bacillus stearothermophilus*. Biochemistry 35:1195–1200

Kawamura S, Tanaka I, Yamasaki N, Kimura M (1997) Contribution of a salt bridge to the thermostability of DNA binding protein HU from *Bacillus stearothermophilus* determined by site-directed mutagenesis. J Biochem 121:448–455

Koradi R, Billeter M, Wuthrich K (1996) MOLMOL: a program for display and analysis of macromolecular structures. J Mol Graph 14(51–55):29–32

Kräutler V, van Gunsteren WF, Hünenberger PH (2001) A fast SHAKE algorithm to solve distance constraint equations for small molecules in molecular dynamics simulations. J Comput Chem 22:501–508

Lavoie BD, Shaw GS, Millner A, Chaconas G (1996) Anatomy of a flexer-DNA complex inside a higher-order transposition intermediate. Cell 85:761–771

Li S, Waters R (1998) *Escherichia coli* strains lacking protein HU are UV sensitive due to a role for HU in homologous recombination. J Bacteriol 180:3750–3756

Liao JH, Lin YC, Hsu J, Lee AY, Chen TA, Hsu CH, Chir JL, Hua KF, Wu TH, Hong LJ, Yen PW, Chiou A, Wu SH (2010) Binding and cleavage of *E. coli* HUbeta by the *E. coli* Lon protease. Biophys J 98:129–137

Lyubchenko YL, Shlyakhtenko LS, Aki T, Adhya S (1997) Atomic force microscopic demonstration of DNA looping by GalR and HU. Nucleic Acids Res 25:873–876

Marley J, Lu M, Bracken C (2001) A method for efficient isotopic labeling of recombinant proteins. J Biomol NMR 20:71–75

Oberto J, Drlica K, Rouviere-Yaniv J (1994) Histones, HMG, HU, IHF: Meme combat. Biochimie 76:901–908

Oberto J, Nabti S, Jooste V, Mignot H, Rouviere-Yaniv J (2009) The HU regulon is composed of genes responding to anaerobiosis, acid stress, high osmolarity and SOS induction. PLoS One 4:e4367

Pettijohn DE (1996) The nucleoid *Escherichia coli* and Salmonella, cellular and molecular biology. In: C. Neidhardt (ed) vol I, Washington, DC, pp 158–166

Pontiggia A, Negri A, Beltrame M, Bianchi ME (1993) Protein HU binds specifically to kinked DNA. Mol Microbiol 7:343–350

Ramstein J, Hervouet N, Coste F, Zelwer C, Oberto J, Castaing B (2003) Evidence of a thermal unfolding dimeric intermediate for the *Escherichia coli* histone-like HU proteins: thermodynamics and structure. J Mol Biol 331:101–121

Raves ML, Doreleijer JF, Vis H, Vorgias CE, Wilson KS, Kaptei R (2001) Joint refinement as a tool for thorough comparison between NMR and X-ray data and structures of HU protein. J Biomol NMR 21:235–248

Rizzuti B, Daggett V, Guzzi R, Sportelli L (2004) The early steps in the unfolding of azurin. Biochemistry 43:15604–15609

Rouviere-Yaniv J, Kjeldgaard NO (1979) Native *Escherichia coli* HU protein is a heterotypic dimer. FEBS Lett 106:297–300

Rouviere-Yaniv J, Yaniv M, Germond JE (1979) *E. coli* DNA binding protein HU forms nucleosome like structure with circular double-stranded DNA. Cell 17:265–274

Ruiz-Sanz J, Filimonov VV, Christodoulou E, Vorgias CE, Mateo PL (2004) Thermodynamic analysis of the unfolding and stability of the dimeric DNA-binding protein HU from the hyperthermophilic eubacterium *Thermotoga maritima* and its E34D mutant. Eur J Biochem 271:1497–1507

Serban D, Arcineigas SF, Vorgias CE, Thomas GJ Jr (2003) Structure and dynamics of the DNA-binding protein HU of *B. stearothermophilus* investigated by Raman and ultraviolet-resonance Raman spectroscopy. Protein Sci 12:861–870

Sonavane S, Chakrabarti P (2008) Cavities and atomic packing in protein structures and interfaces. PLoS Comput Biol 4:e1000188

Song K, Kelso C, de los Santos C, Grollman AP, Simmerling C (2007) Molecular simulations reveal a common binding mode for glycosylase binding of oxidatively damaged DNA lesions. J Am Chem Soc 129:14536–14537

Stella S, Falconi M, Lammi M, Gualerzi CO, Pon CL (2006) Environmental control of the in vivo oligomerization of nucleoid protein H-NS. J Mol Biol 355:169–174

Swinger KK, Lemberg KM, Zhang Y, Rice PA (2003) Flexible DNA bending in HU-DNA cocrystal structures. EMBO J 22:3749–3760

Tsilibaris V, Maenhaut-Michel G, Van Melderen L (2006) Biological roles of the Lon ATP-dependent protease. Res Microbiol 157: 701–713

Vis H, Mariani M, Vorgias CE, Wilson KS, Kaptein R, Boelens R (1995) Solution structure of the HU protein from *Bacillus stearothermophilus*. J Mol Biol 254:692–703

Vranken WF, Boucher W, Stevens TJ, Fogh RH, Pajon A, Llinas M, Ulrich EL, Markley JL, Ionides J, Laue ED (2005) The CCPN data model for NMR spectroscopy: development of a software pipeline. Proteins 59:687–696

Welfle H, Misselwitz R, Welfle K, Schindelin H, Scholtz AS, Heinemann U (1993) Conformations and conformational changes of four Phe→Trp variants of the DNA-binding histone-like protein, HBsu, from *Bacillus subtilis* studied by circular dichroism and fluorescence spectroscopy. Eur J Biochem 217:849–856

White SW, Wilson KS, Appelt K, Tanaka I (1999) The high-resolution structure of DNA-binding protein HU from *Bacillus stearothermophilus*. Acta Crystallogr D Biol Crystallogr 55:801–809

Wilson KS, Vorgias CE, Tanaka I, White SW, Kimura M (1990) The thermostability of DNA-binding protein HU from bacilli. Protein Eng 4:11–22

Wishart DS, Sykes DD (1994) The 13C Chemical-Shift Index: a simple method for the identification of protein secondary structure using 13C chemical-shift data. J Biomol NMR 4:171–180

Wishart DS, Bigam CG, Yao J, Frits Abildgaard F, Dyson HJ, Oldfield E, Markley JL, Sykes BD (1995) 1H, 13C and 15 N chemical shift referencing in biomolecular NMR. J Biomol NMR 6:135–140